Effect of substrate orientation on homoepitaxial growth of β-Ga_2O_3 by halide vapor phase epitaxy

Applied Physics Letters

Effect of substrate orientation on homoepitaxial growth of β-Ga_2O_3 by halide vapor phase epitaxy

Cite as: Appl. Phys. Lett. **120**, 102102 (2022); https://doi.org/10.1063/5.0087609
Submitted: 07 February 2022 • Accepted: 22 February 2022 • Published Online: 10 March 2022

Ken Goto, Hisashi Murakami, Akito Kuramata, et al.

Applied Physics Letters ARTICLE scitation.org/journal/apl

Effect of substrate orientation on homoepitaxial growth of β-Ga_2O_3 by halide vapor phase epitaxy

Cite as: Appl. Phys. Lett. **120**, 102102 (2022); doi: 10.1063/5.0087609
Submitted: 7 February 2022 · Accepted: 22 February 2022 ·
Published Online: 10 March 2022

Ken Goto,[1,a] Hisashi Murakami,[1,2] Akito Kuramata,[3] Shigenobu Yamakoshi,[3] Masataka Higashiwaki,[4] and Yoshinao Kumagai[1,2,a]

AFFILIATIONS

[1]Department of Applied Chemistry, Tokyo University of Agriculture and Technology, Koganei, Tokyo 184-8588, Japan
[2]Institute of Global Innovation Research, Tokyo University of Agriculture and Technology, Koganei, Tokyo 184-8588, Japan
[3]Novel Crystal Technology, Inc., Sayama, Saitama 350-1328, Japan
[4]National Institute of Information and Communications Technology, Koganei, Tokyo 184-8795, Japan

Note: This paper is part of the APL Special Collection on Wide- and Ultrawide-Bandgap Electronic Semiconductor Devices.
[a]**Authors to whom correspondence should be addressed:** gotoken@go.tuat.ac.jp and 4470kuma@cc.tuat.ac.jp

ABSTRACT

The influence of substrate orientation on homoepitaxial growth of beta-gallium oxide by halide vapor phase epitaxy was investigated. Substrates were cut at various angles Δ_b from the (001) plane ($\Delta_b = 0°$) to the (010) plane ($\Delta_b = 90°$) of bulk crystals grown by the edge-defined film-fed growth method. The growth rate increased with increasing absolute value of Δ_b near the (001). However, from the (001) to the (010), as Δ_b increased, the growth rate decreased sharply, and streaky grooves observed in the grown layer on the (001) substrate became triangular pits. The length of the pits decreased with increasing Δ_b, and a pit-free homoepitaxial layer grew at $\Delta_b \approx 60°$. The valley line of the pits was parallel to the [010] direction; therefore, the length of the pits decreased with increasing Δ_b. In addition, transmission electron microscopy observations of the deepest part of a pit revealed that the pits originate from dislocations propagating in the substrate at an angle of 60° with respect to the (001) plane. Therefore, pits are not formed on the grown layer surface when the Δ_b of the substrate is ~60°, because its surface is substantially parallel to the dislocations. The homoepitaxial growth of a pit-free layer on the (011) substrate ($\Delta_b = 61.7°$) was demonstrated, and void defects and dislocations in the substrate were confirmed by the etch-pit method to not be inherited by the homoepitaxial layer.

Gallium oxide (Ga_2O_3) is attracting attention as an ultra-wide-bandgap semiconductor material suitable for next-generation power devices and is expected to provide an energy-saving effect because of its high breakdown electric field strength (> 7 MV/cm)[1,2] predicted on the basis of its large bandgap (4.5 eV or greater).[3,4] Ga_2O_3 has five polymorphs: the α, β, γ, δ, and κ (also referred to as ε) phases.[5,6] Among them, the β phase, which is the most thermally stable, has an advantage in that it can be prepared as large bulk crystals with high crystallinity via melt-growth methods such as the floating zone,[7] Czochralski,[8,9] vertical Bridgman,[10] and edge-defined film-fed growth (EFG)[11,12] methods. Dislocation densities in the bulk substrates, as evaluated by counting the number of etch pits formed by hot alkaline[13] or acidic[14] solutions have been reported to be on the order of 10^3–10^5 cm^{-2} irrespective of the growth method. In addition, intentional doping with Si or Sn provides n-type conductive substrates with extremely low resistivity, which are used in the development of vertical devices. Four inch-diameter substrates prepared by the EFG method have recently been commercialized.[12] The availability of such high-quality substrates has accelerated the development of homoepitaxial growth techniques[15–20] to meet the requirements for drift layers of β-Ga_2O_3-based vertical power devices.

Vertical Schottky barrier diodes (SBDs), which are one of the most suitable applications for β-Ga_2O_3 homoepitaxial substrates, require thick homoepitaxial (drift) layers (~10 μm) with low carrier density. They are often prepared on (001) β-Ga_2O_3 substrates by halide vapor phase epitaxy (HVPE),[21–25] because HVPE enables high-rate homoepitaxial growth of high-purity single-crystal layers and also enables the carrier density to be controlled in the range 10^{15}–10^{18} cm^{-3} by Si doping.[26] However, because grooves and pits are formed on the surfaces of the homoepitaxial layers,[16] chemical mechanical polishing (CMP) of the surface is indispensable for surface planarization before the devices are fabricated.[23,27] In addition to

grooves and pits, defects and/or dislocations in the substrates inherited by the homoepitaxial layer adversely affect SBD performance and yield.[14,28–30] Therefore, elucidating the formation mechanism for the grooves and pits on homoepitaxial layer surfaces and reducing the density of defects and/or dislocations in homoepitaxial layers are critical for improving the performance and yield of devices; however, little research on these topics has been reported.

In the present study, β-Ga_2O_3 was homoepitaxially grown by HVPE on substrates with various orientations. The optimum substrate orientation for which defects and/or dislocations in the substrate do not affect the homoepitaxial layer was then investigated.

The angle formed by [010] and the substrate surface is defined as Δ_b. β-Ga_2O_3 substrates having various orientations between (001) ($\Delta_b = 0°$) and (010) ($\Delta_b = 90°$) were cut from bulk crystals grown in the [010] direction by the EFG method,[12] and the surface was subsequently subjected to CMP. The prepared substrate was loaded into a horizontal atmospheric-pressure hot-wall HVPE reactor[16,26] with a multizone electric furnace for controlling the temperatures of the source zone (the upstream region of the reactor) and the growth zone (the downstream region of the reactor) separately. The source zone was maintained at 850 °C, where gallium monochloride (GaCl) gas was generated by the reaction of Ga metal (6N grade) with Cl_2 gas introduced over Ga. The GaCl gas was transported to the growth zone by purified N_2 carrier gas (dew point < -110 °C), where it reacted with separately supplied O_2 gas to grow β-Ga_2O_3 on the substrate. In the present study, the growth-zone temperature was fixed at 1000 °C. The total gas flow rate was 1600 sccm. The input partial pressure of GaCl (P^o_{GaCl}) was 5.0×10^{-4} or 1.0×10^{-3} atm, and the input partial pressure of O_2 ($P^o_{O_2}$) was adjusted to maintain an input VI/III ratio ($2P^o_{O_2}/P^o_{GaCl}$) of 10.

The growth rate was estimated by determining the thickness of the homoepitaxial layer on the basis of the change in the substrate weight before and after the growth, as measured using an electronic balance with a verification scale interval of 1 μg. The surface morphology was investigated using Nomarski differential interference contrast (NDIC) and confocal violet laser three-dimensional (3D) profile microscopes. In particular, the shapes and depths of the grooves and pits were analyzed by the confocal violet laser 3D profile microscope with a Z-axis measurement resolution of 0.01 μm. In addition, the origin of the pits formed on the surface of the grown layer was investigated using plan-view and cross-sectional bright-field transmission electron microscopy (TEM) images. The TEM specimens containing the target pits were prepared parallel to the (001) plane for the plan-view observation and perpendicular to the [100] axis for the cross section observation using focused-ion-beam processing. To clarify defects and/or dislocations in the substrates used and the homoepitaxially grown layers, the samples were dipped in an 85 wt. % H_3PO_4 aqueous solution at 140 °C for 25 min,[28] and the pits formed on the surfaces were observed using an NDIC microscope.

First, homoepitaxial growth was carried out at $P^o_{GaCl} = 5.0 \times 10^{-4}$ atm for 1 h, and the Δ_b dependence of the growth rate was investigated; the results are shown in Fig. 1. As shown in Fig. 1(b), when Δ_b was $-1.4°$ to $0.8°$ [i.e., in the vicinity of (001)], the growth rate reached its minimum near $\Delta_b = 0°$ and increased as the absolute value of Δ_b increased. This result is attributed to be due to the mirror symmetry of the β-Ga_2O_3 crystal structure ($C2/m$) and increases in the step density at the substrate surface with increasing Δ_b value.

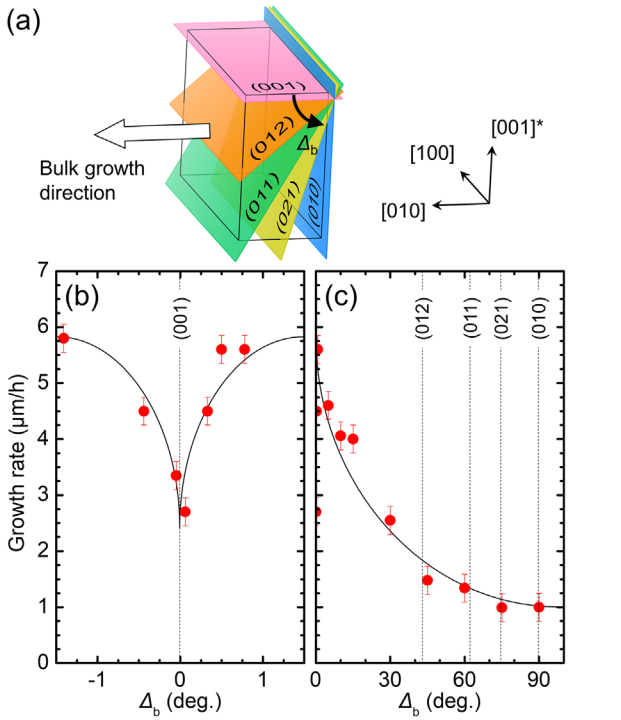

FIG. 1. (a) Schematic of preparation of substrates with various orientations from EFG-grown bulk crystals by varying Δ_b between (001) and (010). The Δ_b dependence of the growth rate (b) near the (001) and (c) over a wide range from (001) to (010). The solid lines are guides for the eyes.

Similar results have been reported for the homoepitaxial growth of β-Ga_2O_3 by molecular beam epitaxy (MBE).[31] Figure 1(c) shows the homoepitaxial growth rate for β-Ga_2O_3 on each substrate between (001) and (010). When Δ_b was greater than 0.8°, the growth rate decreased sharply with increasing Δ_b. This result differs from that in the report by MBE, where the highest homoepitaxial growth rate was obtained on the (010) substrate.[15] The difference in the orientation dependence of the growth rate between HVPE and MBE is likely due to the difference in the source gas molecules and/or the difference in the orientation dependence of the adsorption coefficient for the source gas molecules on the growing surface. The details should be clarified in a future study.

Figure 2 shows the surface NDIC microscopy images of the homoepitaxial layers grown at $P^o_{GaCl} = 5.0 \times 10^{-4}$ atm for 1 h on various substrates with different Δ_b values. On the nominally just (001) substrate ($\Delta_b = 0.06°$), shallow streaky grooves along the [010] direction were formed, consistent with a previous report;[16] however, the grooves changed to triangular pits with increasing absolute value of Δ_b. Here, the directions of the triangular pits were reversed, with $\Delta_b = 0°$ as the boundary, which is attributed to the crystal symmetry of β-Ga_2O_3 as discussed in Fig. 1(b). In addition, as Δ_b increased, the length of the triangular pits decreased; when Δ_b exceeded 45°, the pits became difficult to recognize by NDIC microscopic observation. Interestingly, a pit-free surface was obtained at $\Delta_b \approx 60°$. When Δ_b was 75° or greater, small dots were observed but were hillocks. The morphological change from pit formation to hillock formation was

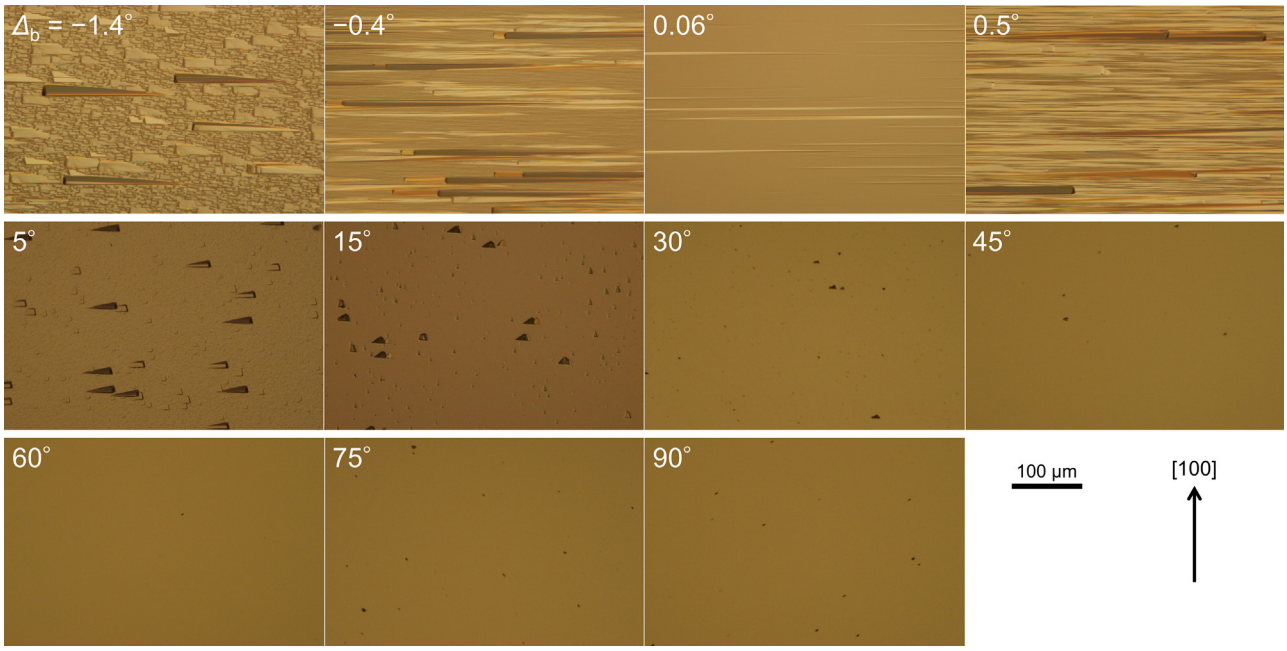

FIG. 2. Surface NDIC microscopy images of homoepitaxial layers grown for 1 h on various substrates with different Δ_b values.

outside the scope of the present study and was not investigated further. However, elucidating the mechanism by which the pit length decreases as Δ_b increases is the key to pit-free homoepitaxial layer growth and is investigated in detail as follows.

The images of triangular pits on the surface of the homoepitaxial layers grown for 1 h on the substrates with a Δ_b of $-1.4°$ and 5° and their cross-sectional profiles obtained using confocal violet laser 3D profile microscopy are shown in Fig. 3. The pits that resemble triangles in the NDIC microscopy images were found to actually be inverted triangular pyramids, and the direction of the valley line was found to differ depending on whether Δ_b is negative or positive (when Δ_b is $-1.4°$ and 5°, the valley line rises to the right and left, respectively). The inclination angle θ of the valley line was calculated from the cross-sectional profile using the following formula:

$$\theta = \tan^{-1}\left(\frac{d}{l}\right), \tag{1}$$

where d is the depth of the pit and l is the length of the pit (l is negative when the pit is pointing to the right and positive when it is pointing to the left). The obtained θ value is approximately equal to the value of Δ_b for each substrate, which indicates that the pits are formed so that the valley lines are parallel to the [010] axis. However, Eq. (1) means that the homoepitaxial layer becomes pit-free ($l = 0$) at $\theta = 90°$ [$\Delta_b = 90°$, i.e., (010)], which is inconsistent with the observation that the pit-free layer was obtained at a Δ_b of ~60° in Fig. 2. Therefore, the results suggest that other factors are responsible for the pit-free homoepitaxial layer being obtained with a Δ_b of ~60°. Notably, the depth of the pit, d, is similar to the thickness of the grown layer. Therefore, the deepest part of the pit reaches the interface between the substrate and the homoepitaxial layer. In addition, the pit density on the grown layer surface was estimated from Fig. 2 to be 10^3–10^4 cm^{-2}, which is almost the same as the dislocation density in the bulk β-Ga_2O_3 crystals used in the present study. From these results, it was inferred that the pits formed on the homoepitaxial layer surface were related to dislocations in the initial substrate.

Figure 4 shows the results of the TEM analysis of the vicinity of the deepest part of the pit formed on the surface of the homoepitaxial

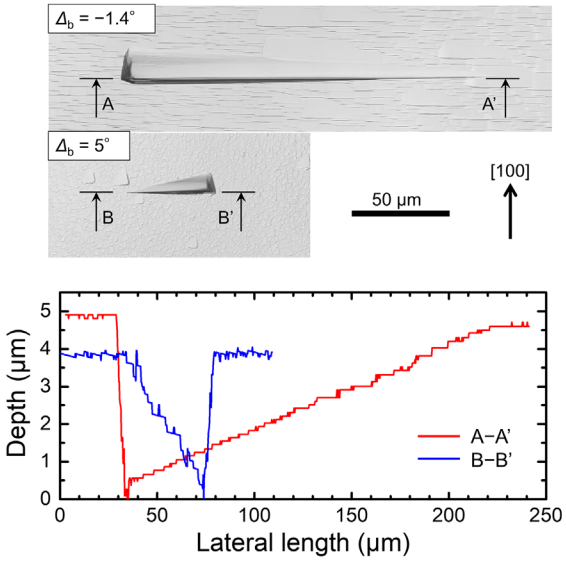

FIG. 3. (Top) Confocal violet laser 3D profile microscopy images of pits on homoepitaxial layers grown for 1 h on substrates with a Δ_b of $-1.4°$ and 5°; (bottom) cross-sectional profiles corresponding to the A–A′ and B–B′ lines.

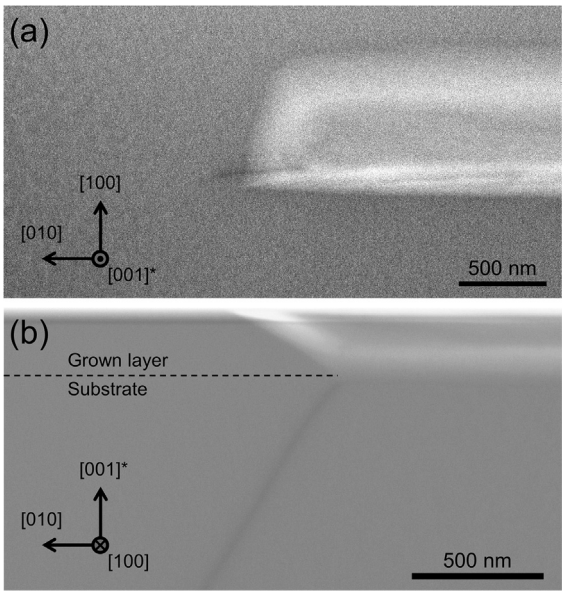

FIG. 4. (a) Plan-view and (b) cross-sectional bright-field TEM images near the bottom of the pit formed on the surface of the homoepitaxial layer grown on the substrate with $\Delta_b = -1.4°$.

layer grown on the substrate with $\Delta_b = -1.4°$. From the plan-view TEM image in Fig. 4(a), the presence of a dislocation was confirmed near the deepest part of the pit. In addition, Fig. 4(b) shows a cross-sectional TEM image of the sample sliced perpendicular to the [100] axis to include the dislocation observed in Fig. 4(a); the image in Fig. 4(b) clearly shows that this dislocation propagates from the substrate and that the point where the dislocation reaches the substrate surface is the starting point of pit formation. The threading dislocations in a β-Ga_2O_3 bulk crystal grown in the [010] direction by EFG have been reported to propagate on slip planes,[32,33] and Yao *et al.* confirmed that {100} is one of the slip planes.[33] The result in Fig. 4(b) is consistent with that reported by Yao *et al.* Here, the dislocation is at an angle of ~60° with respect to the (001) plane; i.e., for the substrate with a Δ_b of ~60° [near the (011) plane], dislocations propagate substantially parallel to the substrate surface and do not appear on the substrate surface. This result explains why a pit-free homoepitaxial layer was realized on the substrate with $\Delta_b \approx 60°$ (Fig. 2).

To verify the aforementioned model, a (011) substrate ($\Delta_b = 61.7°$) and a (001) substrate ($\Delta_b = 0.04°$) were prepared, and defects or dislocations on their surfaces were evaluated by etching using a hot H_3PO_4 solution after substrate preparation and after CMP of the homoepitaxial layer surface. Two types of pits, bullet-shaped and rectangular-shaped, were formed on the (001) substrate [Fig. 5(a)], and these pits are considered to have originated from dislocations and voids, respectively.[14,28] By contrast, no etch pits were formed on the (011) substrate [Fig. 5(d)]. This also explains why dislocations are not observed on the surface of the (011) substrate. Figures 5(b) and 5(e) show the surfaces after an 8 μm thick homoepitaxial layer was grown on each substrate. In this experiment, homoepitaxial growth was performed at $P^o_{GaCl} = 1.0 \times 10^{-3}$ atm, which is twice the P^o_{GaCl} used in previous experiments, and the growth rates on the (001) and (011) substrates were 4.8 and 2.8 μm/h, respectively. Each value is approximately twice the growth rate shown in Figs. 1(b) and 1(c). In the homoepitaxial layer grown on the (001) substrate, streaky grooves along the [010] direction were formed on the surface [Fig. 5(b)], whereas the homoepitaxial layer grown on the (011) substrate exhibited a smooth surface with no pits or hillocks even when the growth rate was increased [Fig. 5(e)]. Because the depth of the streaky grooves on the surface of the homoepitaxial layer grown on the (001) substrate was ~20% of the grown layer thickness, the surface of the homoepitaxial

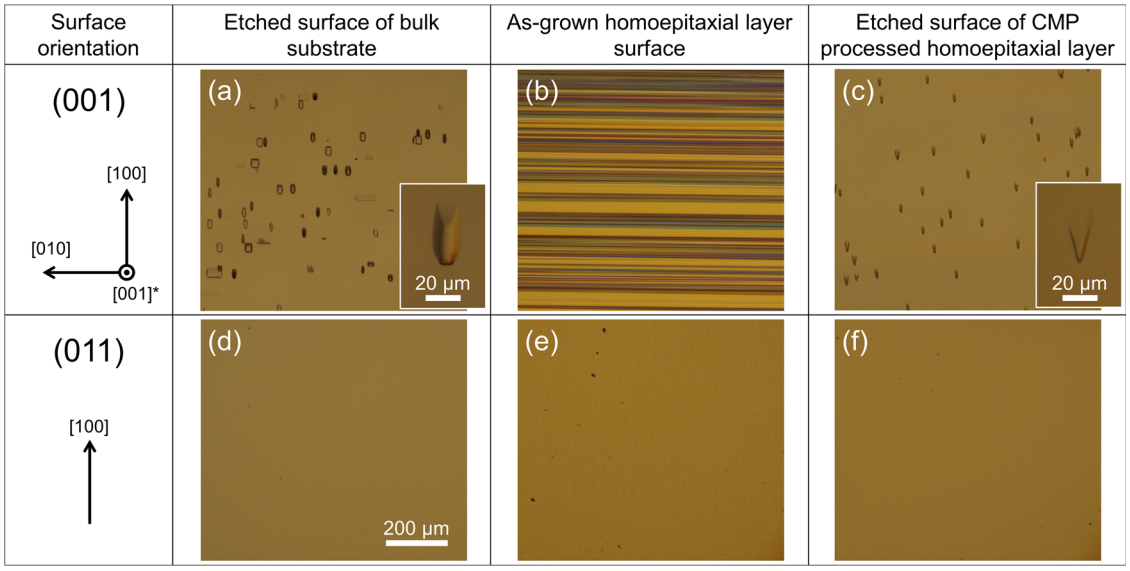

FIG. 5. NDIC microscopy images of (a)–(c) (001) and (d)–(f) (011) substrate surfaces: (a) and (d) after the substrate was etched with a hot H_3PO_4 solution, (b) and (e) after an 8 μm-thick homoepitaxial layer was grown, and (c) and (f) after a CMP-processed homoepitaxial layer was etched with a hot H_3PO_4 solution. The insets in (a) and (c) are magnified images of a typical etch pit.

layer on both substrates was flattened by removing 3 μm by CMP; etch pits were then formed for each layer by etching [Figs. 5(c) and 5(f)]. As shown in Fig. 5(c), only chevron-shaped pits were observed on the homoepitaxial layer surface grown on the (001) substrate. A comparison of the density of the etch pits with the density observed in Fig. 5(a) suggests that, like the bullet-shaped pits formed on the substrate surface, the chevron-shaped pits originated from dislocations in the homoepitaxial layer. Although further investigation is needed in the future, it is found that the voids in the substrate do not propagate to the homoepitaxial layer. By contrast, no etch pits were formed on the homoepitaxial layer grown on the (011) substrate [Fig. 5(f)], suggesting that no dislocations were present in the homoepitaxial layer. Therefore, adopting the (011) β-Ga_2O_3 substrate led to an improvement in the crystallinity of the homoepitaxial layer. It is expected that the performance and yield of power devices fabricated using this layer will be improved.

In summary, homoepitaxial growth of β-Ga_2O_3 by atmospheric-pressure HVPE was investigated on substrates cut at various angles Δ_b from the (001) plane ($\Delta_b = 0°$) to the (010) plane ($\Delta_b = 90°$) of bulk β-Ga_2O_3 crystals grown in the [010] direction by the EFG method. In the vicinity of the (001) substrate, the lowest growth rate was obtained for a Δ_b of 0° and the growth rate increased with a slight increase in the absolute value of Δ_b. However, from (001) to (010), the growth rate decreased sharply with increasing Δ_b. At the same time, streaky grooves on the surface of the homoepitaxial layer on a (001) substrate changed to inverted triangular pits (pyramids). Because the valley line of the triangular pits was parallel to [010], the length of the pits decreased with increasing Δ_b. Homoepitaxial layers without pits grew when Δ_b was higher than 60°. TEM observations near the deepest part of the pit revealed that the origin of the pit is dislocations in the substrate propagating at an angle of 60° with respect to the (001) plane. At $\Delta_b \approx 60°$, the surface of the substrate was found to be substantially parallel to the dislocations; thus, pits were not formed on the surface of the grown layer. On the basis of these findings, homoepitaxial growth of a pit-free layer on the (011) β-Ga_2O_3 substrate with $\Delta_b = 61.7°$ was demonstrated, and voids and dislocations in the substrate were confirmed to not have been inherited by the homoepitaxial layer. In the future, if n-type conductivity control by Si doping becomes possible on (011) β-Ga_2O_3 substrates as well as on (001) substrates, then (011) substrates might become one of the choices for the development of β-Ga_2O_3-based power devices. The use of (010) substrates may also be desirable as they provide a smooth homoepitaxial layer surface, although perhaps dislocations are present.

Part of this work was supported by the Council for Science, Technology, and Innovation (CSTI), the Cross-ministerial Strategic Innovation Promotion Program (SIP), "Next-generation power electronics" (funding agency: NEDO), and the Institute of Global Innovation Research, Tokyo University of Agriculture and Technology, Japan.

AUTHOR DECLARATIONS

Conflict of Interest

The authors have no conflicts of interest to disclose.

DATA AVAILABILITY

The data that support the findings of this study are available within the article.

REFERENCES

[1]M. Higashiwaki, K. Sasaki, A. Kuramata, T. Masui, and S. Yamakoshi, Appl. Phys. Lett. **100**, 013504 (2012).
[2]Z. Xia, H. Chandrasekar, W. Moore, C. Wang, A. J. Lee, J. McGlone, N. K. Kalarickal, A. Arehart, S. Ringel, F. Yang, and S. Rajan, Appl. Phys. Lett. **115**, 252104 (2019).
[3]H. H. Tippins, Phys. Rev. **140**, A316 (1965).
[4]T. Onuma, S. Saito, K. Sasaki, T. Masui, T. Yamaguchi, T. Honda, and M. Higashiwaki, Jpn. J. Appl. Phys., Part 1 **54**, 112601 (2015).
[5]R. Roy, V. G. Hill, and E. F. Osborn, J. Am. Chem. Soc. **74**, 719 (1952).
[6]I. Cora, F. Mezzadri, F. Boschi, M. Bosi, M. Čaplovičová, G. Calestani, I. Dódony, B. Pécz, and R. Fornari, CrystEngComm **19**, 1509 (2017).
[7]E. G. Víllora, K. Shimamura, Y. Yoshikawa, K. Aoki, and N. Ichinose, J. Cryst. Growth **270**, 420 (2004).
[8]Z. Galazka, K. Irmscher, R. Uecker, R. Bertram, M. Pietsch, A. Kwasniewski, M. Naumann, T. Schulz, R. Schewski, D. Klimm, and M. Bickermann, J. Cryst. Growth **404**, 184 (2014).
[9]J. D. Blevins, K. Stevens, A. Lindsey, G. Foundos, and L. Sande, IEEE Trans. Semicond. Manuf. **32**, 466 (2019).
[10]E. Ohba, T. Kobayashi, T. Taishi, and K. Hoshikawa, J. Cryst. Growth **556**, 125990 (2021).
[11]H. Aida, K. Nishiguchi, H. Takeda, N. Aota, K. Sunakawa, and Y. Yaguchi, Jpn. J. Appl. Phys., Part 1 **47**, 8506 (2008).
[12]A. Kuramata, K. Koshi, S. Watanabe, Y. Yamaoka, T. Masui, and S. Yamakoshi, Jpn. J. Appl. Phys., Part 1 **55**, 1202A2 (2016).
[13]Y. Yao, Y. Ishikawa, and Y. Sugawara, Phys. Status Solidi A **217**, 1900630 (2020).
[14]M. Kasu, K. Hanada, T. Moribayashi, A. Hashiguchi, T. Oshima, T. Oishi, K. Koshi, K. Sasaki, A. Kuramata, and O. Ueda, Jpn. J. Appl. Phys., Part 1 **55**, 1202BB (2016).
[15]K. Sasaki, A. Kuramata, T. Masui, E. G. Víllora, K. Shimamura, and S. Yamakoshi, Appl. Phys. Express **5**, 035502 (2012).
[16]H. Murakami, K. Nomura, K. Goto, K. Sasaki, K. Kawara, Q. T. Thieu, R. Togashi, Y. Kumagai, M. Higashiwaki, A. Kuramata, S. Yamakoshi, B. Monemar, and A. Koukitu, Appl. Phys. Express **8**, 015503 (2015).
[17]S.-D. Lee, K. Kaneko, and S. Fujita, Jpn. J. Appl. Phys., Part 1 **55**, 1202B8 (2016).
[18]K. D. Leedy, K. D. Chabak, V. Vasilyev, D. C. Look, J. J. Boeckl, J. L. Brown, S. E. Tetlak, A. J. Green, N. A. Moser, A. Crespo, D. B. Thomson, R. C. Fitch, J. P. McCandless, and G. H. Jessen, Appl. Phys. Lett. **111**, 012103 (2017).
[19]S. Rafique, M. R. Karim, J. M. Johnson, J. Hwang, and H. Zhao, Appl. Phys. Lett. **112**, 052104 (2018).
[20]M. Baldini, M. Albrecht, A. Fiedler, K. Irmscher, R. Schewski, and G. Wagner, ECS J. Solid State Sci. Technol. **6**, Q3040 (2017).
[21]M. Higashiwaki, K. Konishi, K. Sasaki, K. Goto, K. Nomura, Q. T. Thieu, R. Togashi, H. Murakami, Y. Kumagai, B. Monemar, A. Koukitu, A. Kuramata, and S. Yamakoshi, Appl. Phys. Lett. **108**, 133503 (2016).
[22]K. Konishi, K. Goto, H. Murakami, Y. Kumagai, A. Kuramata, S. Yamakoshi, and M. Higashiwaki, Appl. Phys. Lett. **110**, 103506 (2017).
[23]J. Yang, S. Ahn, F. Ren, S. J. Pearton, S. Jang, J. Kim, and A. Kuramata, Appl. Phys. Lett. **110**, 192101 (2017).
[24]W. Li, Z. Hu, K. Nomoto, Z. Zhang, J.-Y. Hsu, Q. T. Thieu, K. Sasaki, A. Kuramata, D. Jena, and H. G. Xing, Appl. Phys. Lett. **113**, 202101 (2018).
[25]C.-H. Lin, Y. Yuda, M. H. Wong, M. Sato, N. Takekawa, K. Konishi, T. Watahiki, M. Yamamuka, H. Murakami, Y. Kumagai, and M. Higashiwaki, IEEE Electron Device Lett. **40**, 1487 (2019).
[26]K. Goto, K. Konishi, H. Murakami, Y. Kumagai, B. Monemar, M. Higashiwaki, A. Kuramata, and S. Yamakoshi, Thin Solid Films **666**, 182 (2018).
[27]Q. T. Thieu, D. Wakimoto, Y. Koishikawa, K. Sasaki, K. Goto, K. Konishi, H. Murakami, A. Kuramata, Y. Kumagai, and S. Yamakoshi, Jpn. J. Appl. Phys., Part 1 **56**, 110310 (2017).
[28]T. Oshima, A. Hashiguchi, T. Moribayashi, K. Koshi, K. Sasaki, A. Kuramata, O. Ueda, T. Oishi, and M. Kasu, Jpn. J. Appl. Phys., Part 1 **56**, 086501 (2017).
[29]S. Masuya, K. Sasaki, A. Kuramata, S. Yamakoshi, O. Ueda, and M. Kasu, Jpn. J. Appl. Phys., Part 1 **58**, 055501 (2019).

[30]S. Sdoeung, K. Sasaki, K. Kawasaki, J. Hirabayashi, A. Kuramata, T. Oishi, and M. Kasu, Appl. Phys. Lett. **117**, 022106 (2020).
[31]P. Mazzolini, A. Falkenstein, Z. Galazka, M. Martin, and O. Bierwagen, Appl. Phys. Lett. **117**, 222105 (2020).
[32]H. Yamaguchi, A. Kuramata, and T. Masui, Superlattices Microstruct. **99**, 99 (2016).
[33]Y. Yao, Y. Ishikawa, and Y. Sugawara, Jpn. J. Appl. Phys., Part 1 **59**, 125501 (2020).